Experimental validation of optimum input polarization states for Mueller matrix determination with a dual photoelastic modulator polarimeter

Adam Gribble,[1,*] David Layden,[2] and I. Alex Vitkin[1,3,4]

[1]*Department of Medical Biophysics, University of Toronto, 610 University Avenue, Toronto, Ontario M5G 2M9, Canada*

[2]*Department of Physics and Astronomy, University of Waterloo, 200 University Avenue West, Waterloo, Ontario N2L 2G1, Canada*

[3]*Division of Biophysics and Bioimaging, Ontario Cancer Institute, University Health Network, 610 University Avenue, Toronto, Ontario MG5 2M9, Canada*

[4]*Department of Radiation Oncology, University of Toronto, 610 University Avenue, Toronto, Ontario M5G 2M9, Canada*

**Corresponding author: adam.gribble@mail.utoronto.ca*

Received September 2, 2013; revised November 1, 2013; accepted November 6, 2013;
posted November 6, 2013 (Doc. ID 196725); published December 4, 2013

Dual photoelastic modulator polarimeters can measure light polarization, which is often described as a Stokes vector. By evaluating changes in polarization when light interacts with a sample, the sample Mueller matrix also can be derived, completely describing its interaction with polarized light. The choice of which and how many input Stokes vectors to use for sample investigation is under the experimenter's control. Previous work has predicted that sets of input Stokes vectors forming the vertices of platonic solids on the Poincaré sphere allow for the most robust Mueller matrix determination. Further, when errors specific to the dual photoelastic modulator polarimeter are considered, simulations revealed that one specific shape and orientation of Stokes vectors (cube on the Poincaré sphere with vertices away from principal sphere axes) allows for the most robust Mueller matrix determination. Here we experimentally validate the optimum input Stokes vectors for dual photoelastic modulator Mueller polarimetry, toward developing a robust polarimetric platform of increasing relevance to biophotonics.

OCIS codes: (120.5410) Polarimetry; (170.4090) Modulation techniques; (260.5430) Polarization; (230.4110) Modulators.

http://dx.doi.org/10.1364/OL.38.005272

Polarized light is often described by a four-element Stokes vector, $\mathbf{S} = [I, Q, U, V]^T$ where I is the overall intensity, Q and U describe the magnitude and orientation of the linearly polarized component, and V describes the magnitude and handedness of the circularly polarized component [1]. Stokes vectors are often normalized by dividing a factor of I out of each element. For fully polarized light, the equality $(Q/I)^2 + (U/I)^2 + (V/I)^2 = 1$ is satisfied, providing a convenient way to geometrically represent polarization states. If Q/I, U/I, and V/I are used as the axes of a 3D coordinate system, then plots of fully polarized states will produce a sphere of unit radius, centered about the origin. This is known as the Poincaré sphere [2,3]. Partially polarized light satisfies the inequality $(Q/I)^2 + (U/I)^2 + (V/I)^2 < 1$; thus these states lie inside the Poincaré sphere. Random polarization corresponds to the zero vector.

When an initial beam of polarized light, referred to as the input Stokes vector, $\mathbf{S}^{\text{in}}$, interacts with a sample, its polarization state is altered. The emergent light, denoted by the output Stokes vector, $\mathbf{S}^{\text{out}}$, is determined by the sample properties according to the matrix-vector equation

$$\mathbf{S}^{\text{out}} = \mathbf{M}\mathbf{S}^{\text{in}}. \tag{1}$$

Here $\mathbf{M}$ is the sample's Mueller matrix. This polarization fingerprint encodes properties such as depolarization, linear retardance, diattenuation, and optical activity to completely describe the sample's interaction with polarized light [3,4]. Measurement of the 16-element (4×4) Mueller matrix is the goal of Mueller polarimetry. In biophotonics, this technique has been investigated for noninvasive glucose monitoring [5,6], monitoring myocardial infarct response to stem-cell therapies in animals [6,7], detecting axial heterogeneity in anisotropic tissue [8], characterizing distended rat bladders [9], characterizing healthy and cancerous human cervix [10] and colon samples [11], and so on.

To determine the sample Mueller matrix, one measures a set of n input light polarizations, grouped as the matrix $\mathbb{S}^{\text{in}} = [\mathbf{S}^{\text{in}}_{(1)} \ldots \mathbf{S}^{\text{in}}_{(n)}]$, and corresponding output polarizations, $\mathbb{S}^{\text{out}} = [\mathbf{S}^{\text{out}}_{(1)} \ldots \mathbf{S}^{\text{out}}_{(n)}]$. Using these Stokes matrices in place of individual Stokes vectors, n versions of Eq. (1) become

$$\mathbb{S}^{\text{out}} = \mathbf{M}\mathbb{S}^{\text{in}}. \tag{2}$$

A minimum of 16 linear equations, which can be generated from $n = 4$ unique input vectors and their corresponding outputs, are required to solve for the Mueller matrix [12]. Through rearrangement of Eq. (2),

$$\mathbf{M} = \mathbb{S}^{\text{out}}(\mathbb{S}^{\text{in}})^{-1}, \tag{3}$$

provided $\mathbb{S}^{\text{in}}$ is invertible. Supplemental measurements $(n > 4)$ can be made in an attempt to reduce Mueller matrix errors [12]. In this case, the system in Eq. (2) is likely overdetermined, and the least-squares best fit is given by

$$\mathbf{M} = \mathbb{S}^{\text{out}}(\mathbb{S}^{\text{in}})^{+}, \tag{4}$$

where $(\mathbb{S}^{\text{in}})^{+} = (\mathbb{S}^{\text{in}})^T[\mathbb{S}^{\text{in}}(\mathbb{S}^{\text{in}})^T]^{-1}$ is the Moore–Penrose pseudoinverse of $\mathbb{S}^{\text{in}}$ [12].

Unfortunately, the highly turbid nature of biological tissue causes light to undergo multiple scattering events before it is detected, leading to increased depolarization. It is therefore imperative to measure and isolate the

remaining information-carrying polarized fraction of light that emerges from tissue with high accuracy and SNR. This is a goal of the dual photoelastic modulator (dual PEM) polarimetry system (Fig. 1) described by Guan *et al.* [13], which combines polarization modulation with phase-sensitive synchronous detection to accurately measure all four Stokes parameters simultaneously, with no mechanically moving parts.

An important question is whether there exists a specific set of input Stokes vectors that allows for the most robust Mueller matrix determination by a dual PEM system. In a previous theoretical paper [14], Layden *et al.* derived an expression for an upper bound on the root-mean-square (RMS) error in Mueller matrix elements, denoted $\langle \delta \mathbf{M} \rangle$, resulting from random measurement noise, $\delta \mathbb{S}^{\text{in}}$ and $\delta \mathbb{S}^{\text{out}}$, in input and output Stokes vectors, respectively:

$$\langle \delta \mathbf{M} \rangle \lesssim \frac{n^{1/2}}{2} (\langle \delta \mathbb{S}^{\text{out}} \rangle + 4 \langle \mathbf{M} \rangle \langle \delta \mathbb{S}^{\text{in}} \rangle) \| (\mathbb{S}^{\text{in}})^{+} \|, \tag{5}$$

where $\langle \mathbf{A} \rangle$ denotes the RMS of the elements in matrix $\mathbf{A}$, and $\| (\mathbb{S}^{\text{in}})^{+} \|$ is the norm of the pseudoinverse of $\mathbb{S}^{\text{in}}$.

Although noise in Stokes vectors is not directly controllable, the experimenter can choose input vectors to minimize $\| (\mathbb{S}^{\text{in}})^{+} \|$, which in turn minimizes the Mueller error, $\langle \delta \mathbf{M} \rangle$, for fixed n. This occurs when vectors of $\mathbb{S}^{\text{in}}$ form vertices of a Platonic solid when plotted on the Poincaré sphere [14]. For $n = 4$, this is a tetrahedron, $n = 6$ an octahedron, $n = 8$ a cube, and $n = 12$ an icosahedron. The superiority of these arrangements can be understood from the fact that, for a given n, a Platonic configuration allows the Stokes vectors to be spread as far apart as possible on the Poincaré sphere, providing even sampling over the entire polarization space.

However, when a vector set satisfies the Platonic solid condition, the following is true of its pseudoinverse [14]:

$$\| (\mathbb{S}^{\text{in}})^{+} \|_{\min}(n) = \left(\frac{10}{n} \right)^{1/2}. \tag{6}$$

Substituting into Eq. (5),

$$\langle \delta \mathbf{M} \rangle \lesssim \left(\frac{5}{2} \right)^{1/2} (\langle \delta \mathbb{S}^{\text{out}} \rangle + 4 \langle \mathbf{M} \rangle \langle \delta \mathbb{S}^{\text{in}} \rangle). \tag{7}$$

Thus it appears that as long as the input Stokes vectors form vertices of a Platonic solid, neither the number of input vectors, nor the orientation (under rotation) of the solid on the Poincaré sphere, has any first-order effect on Mueller error. To address this lack of specificity, Layden *et al.* [14] considered an error source unique to the dual-PEM system: phase errors.

Phase errors occur when the phase differences between signal oscillations and PEM reference frequencies are measured by the system lock-in amplifiers to be close to 0 or ±180°. This occurs most frequently when signal amplitudes are small, i.e., when $|Q|$, $|U|$, or $|V|$ approach 0. When Stokes vectors near these phase-error regions (see Fig. 2) are measured, noise fluctuations may cause the measured phase to switch signs, leading to a sign error in the corresponding Stokes element. A simulation, modeling the effects of phase errors and random measurement noise, revealed the following set of input Stokes vectors allows for the most robust result [14]:

$$\mathbb{S}^{\text{in}}_{(\text{opt})} = [\mathbf{S}^{\text{in}}_{(1)} \cdots \mathbf{S}^{\text{in}}_{(8)}] \quad \text{where}$$

$$\mathbf{S}^{\text{in}}_{(1)} = \begin{bmatrix} 1 \\ 0.58 \\ 0.58 \\ 0.58 \end{bmatrix}; \quad \mathbf{S}^{\text{in}}_{(2)} = \begin{bmatrix} 1 \\ 0.58 \\ 0.58 \\ -0.58 \end{bmatrix}; \quad \mathbf{S}^{\text{in}}_{(3)} = \begin{bmatrix} 1 \\ 0.58 \\ -0.58 \\ 0.58 \end{bmatrix};$$

$$\mathbf{S}^{\text{in}}_{(4)} = \begin{bmatrix} 1 \\ 0.58 \\ -0.58 \\ -0.58 \end{bmatrix}; \quad \mathbf{S}^{\text{in}}_{(5)} = \begin{bmatrix} 1 \\ -0.58 \\ 0.58 \\ 0.58 \end{bmatrix}; \quad \mathbf{S}^{\text{in}}_{(6)} = \begin{bmatrix} 1 \\ -0.58 \\ 0.58 \\ -0.58 \end{bmatrix};$$

$$\mathbf{S}^{\text{in}}_{(7)} = \begin{bmatrix} 1 \\ -0.58 \\ -0.58 \\ 0.58 \end{bmatrix}; \quad \mathbf{S}^{\text{in}}_{(8)} = \begin{bmatrix} 1 \\ -0.58 \\ -0.58 \\ -0.58 \end{bmatrix}. \tag{8}$$

This "Optimum" set [see Fig. 2(a)] forms a cube ($n = 8$) on the Poincaré sphere, with all vertices oriented as far away as possible from the regions most prone to phase error.

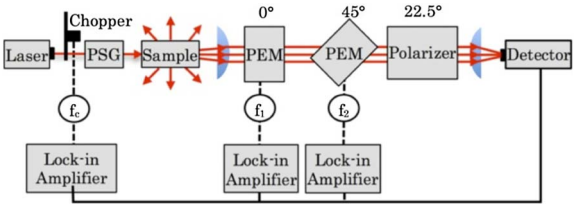

Fig. 1. Dual PEM polarimeter. Polarized light of a suitable input state is produced by the polarization state generator (PSG). This light interacts with a sample, and the output polarization is analyzed by passing through two PEMs (45° and 0° above horizontal) and a linear polarizer (22.5° above horizontal). The modulation frequencies, f_1 and f_2, of the PEMs are used as references for lock-in amplifiers, which recover Q, U, and V of light reaching the detector, via synchronous detection. The I component is recovered by a lock-in using the beam chopper frequency, f_c, as a reference.

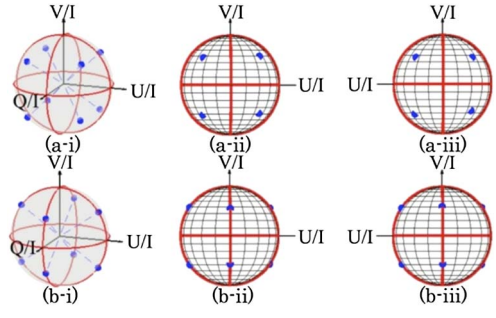

Fig. 2. Sets of input vectors forming Platonic solids (namely, a cube) when plotted on the Poincaré sphere. The sphere equator represents linear polarizations, and the poles represent circular polarizations. Phase-error regions, where Q, U, or $V = 0$, are shown with red circles. (a) The Optimum set contains Stokes vectors that from vertices of a cube, maximally distant from the phase-error regions. (b) The Rotated-Optimum set also forms a cube, but with vertices rotated into the phase-error regions. Column (i) gives 3D views; column (ii) shows the front face of the Poincaré sphere; column (iii) shows the back face.

Here we set out to experimentally test the validity of this Optimum set of input Stokes vectors. The Mueller matrix of a liquid biological phantom was measured with five different sets of input polarizations. The Mueller error associated with each set was then quantified.

Measurements were made in transmission with a 660 nm laser (Coherent Cube 660-60C). Due to multiple scattering, the path length (thru 2 mm × 10 mm × 43 mm cuvette) is greater than 2 mm, and coherence effects are negligible.

The sample had properties of porcine liver tissue (reduced scattering coefficient, $\mu_s' = 5.60\ \text{cm}^{-1}$, and absorption coefficient, $\mu_a = 4.14\ \text{cm}^{-1}$) [15]. We chose a sample that only exhibits depolarization, since it is the dominant polarization effect in biological tissue. Linear birefringence is next, and circular birefringence is weakest. The relative strengths of these, and other rare effects (i.e., diattenuation), are tissue and wavelength dependent.

The Mueller matrix, calculated from Eq. (4) using the Optimum set measurements, was

$$\mathbf{M}_{(0)} = \begin{bmatrix} 1.000 & 0.0000 & 0.0000 & 0.0000 \\ -0.0076 & -0.4147 & 0.0011 & 0.0005 \\ -0.0050 & -0.0004 & 0.4355 & 0.0007 \\ 0.0037 & 0.0032 & 0.0016 & 0.8220 \end{bmatrix}. \quad (9)$$

Each of the five sets of input polarizations consisted of $n = 8$ different Stokes vectors. The Optimum set, Fig. 2(a), contains vectors forming vertices of a cube when plotted on the Poincaré sphere, with vertices maximally distant from the phase-error regions. The second set, Fig. 2(b), also forms vertices of a cube, allowing for an even sampling of the polarization space. However, this "Rotated-Optimum" set is oriented away from its optimum configuration so that the vectors approach the phase-error regions.

The three remaining sets, shown in Fig. 3, consist of Stokes vectors produced by random polarization state generator (PSG) orientations (i.e., random polarizer and quarter-wave plate orientations). These "Random" sets differ in how evenly distributed their polarization vectors are, as well as in proximity to the phase-error regions. In order to quantify these different characteristics we define: (1) the "mean separation angle" between the eight Stokes vectors as a measure of a set's "spread" and (2) the number of normalized Stokes elements (out of 24—Q, U, and V for eight vectors) in each set with magnitude <0.10 as a measure of a set's proximity to the phase-error regions. These characteristics are summarized in Table 1. For vectors forming vertices of a perfect cube, the mean angle between vectors is a maximum, at 102.9°. As this mean separation angle decreases, the plotted Stokes vectors become less spread out (become more clustered) and less resemble the vertices of a cube. As seen in Table 1, Optimum and Rotated-Optimum sets have mean separation angles close to the ideal 102.9°, whereas those of the Random sets are lower. Random3 has the most clustered input Stokes vectors, with a mean separation angle of 90.4°. The Optimum set best avoids the phase-error regions, Rotated-Optimum is the worst overall, and Random3 is worst among the Random sets.

To characterize the error associated with a set of input Stokes vectors, we first measured each of its eight input

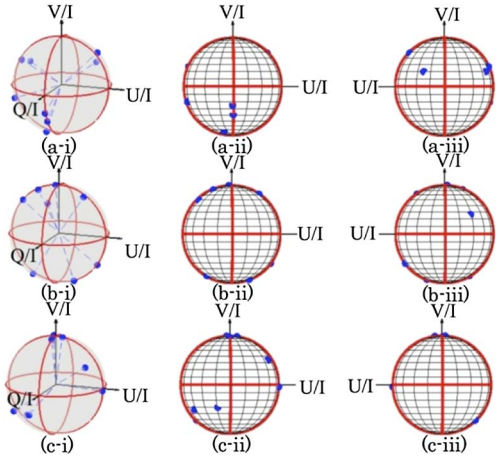

Fig. 3. Random sets of input Stokes vectors plotted on the Poincaré sphere. Sets differ in mean separation angle and proximity to phase-error regions: (a) Random1; (b) Random2; (c) Random3. Column (i) gives 3D views; column (ii) shows the front face of the Poincaré sphere; column (iii) shows the back face.

Stokes vectors, $\mathbf{S}_{(ij)}^{\text{in}}$ ($i = 1$ to 8), with the dual PEM setup, and each input vector was repeatedly measured 10 times, ($j = 1$ to 10) for a total of 80 input Stokes vector measurements. The tissue phantom was then placed in the beam path, and the eight corresponding output states, $\mathbf{S}_{(ij)}^{\text{out}}$, were measured, again with 10 measurements of each vector. As a result, each data set contained 160 Stokes vector measurements. ($\mathbf{S}_{(1\,1)}^{\text{in}}$ to $\mathbf{S}_{(8\,10)}^{\text{in}}$ and $\mathbf{S}_{(1\,1)}^{\text{out}}$ to $\mathbf{S}_{(8\,10)}^{\text{out}}$). A "correct" reference Mueller matrix for the tissue phantom, $\mathbf{M}_{(0)}$, was calculated for the set, from Eq. (4), using the eight average input vectors, $\mathbb{S}_{(\text{avg})}^{\text{in}} = [\mathbf{S}_{(1\,\text{avg})}^{\text{in}} \cdots \mathbf{S}_{(8\,\text{avg})}^{\text{in}}]$, and eight corresponding average output vectors, $\mathbb{S}_{(\text{avg})}^{\text{out}} = [\mathbf{S}_{(1\,\text{avg})}^{\text{out}} \cdots \mathbf{S}_{(8\,\text{avg})}^{\text{out}}]$, where

$$\mathbf{S}_{(i\,\text{avg})} = \frac{\sum_{j=1}^{10} \mathbf{S}_{(ij)}}{10}. \quad (10)$$

To get a quantitative measure of how individual Stokes measurements affected the stability of the inferred Mueller matrix, $\mathbf{M}_{(0)}$, we calculated 160 "erroneous" Mueller matrices, $\mathbf{M}_{(k)}$, where $k = 1$ to 160. Each $\mathbf{M}_{(k)}$ was found using one individual (as opposed to averaged) Stokes vector measurement, $\mathbf{S}_{(ij)}$, and the average Stokes vectors for the remaining 15 input/output states. For example, $\mathbf{M}_{(1)}$ was found from $\mathbb{S}^{\text{in}} = [\mathbf{S}_{(1\,1)}^{\text{in}} \mathbf{S}_{(2\,\text{avg})}^{\text{in}} \cdots \mathbf{S}_{(8\,\text{avg})}^{\text{in}}]$ and $\mathbb{S}_{(\text{avg})}^{\text{out}}$; $\mathbf{M}_{(2)}$ from $\mathbb{S}^{\text{in}} = [\mathbf{S}_{(1\,2)}^{\text{in}} \mathbf{S}_{(2\,\text{avg})}^{\text{in}} \cdots \mathbf{S}_{(8\,\text{avg})}^{\text{in}}]$ and $\mathbb{S}_{(\text{avg})}^{\text{out}}$;

Table 1. Characteristics of Input Polarization Sets

Input Stokes Vectors	Mean Separation Angle (degrees)[a]	Stokes Elements Near Phase-Error Regions[b]
Optimum	102.3	0
Rotated-Optimum	102.6	8
Random1	94.2	2
Random2	97.8	3
Random3	90.4	5

[a]102.9° for a perfect cube. Smaller angles are more clustered. Optimum and Rotated-Optimum are not exactly 102.9° due to experimental imperfections.

[b]Number of elements (out of 24) in $\mathbb{S}_{(\text{avg})}^{\text{in}}$ with magnitude <0.10.

$\mathbf{M}_{(11)}$ from $\mathbb{S}^{\text{in}} = [\mathbf{S}^{\text{in}}_{(1\,\text{avg})}\mathbf{S}^{\text{in}}_{(2\,1)}\mathbf{S}^{\text{in}}_{(3\,\text{avg})}\cdots\mathbf{S}^{\text{in}}_{(8\,\text{avg})}]$ and $\mathbb{S}^{\text{out}}_{(\text{avg})}$; and $\mathbf{M}_{(160)}$ from $\mathbb{S}^{\text{in}}_{\text{avg}}$ and $\mathbb{S}^{\text{out}} = [\mathbf{S}^{\text{out}}_{(1\,\text{avg})}\cdots\mathbf{S}^{\text{out}}_{(7\,\text{avg})}\mathbf{S}^{\text{out}}_{(8\,10)}]$. The difference matrix for each $\mathbf{M}_{(k)}$ was calculated as

$$\delta\mathbf{M}_{(k)} = \mathbf{M}_{(k)} - \mathbf{M}_{(0)}, \tag{11}$$

and the error in each $\mathbf{M}_{(k)}$ is defined as the RMS of $\delta\mathbf{M}_{(k)}$:

$$\langle\delta\mathbf{M}_{(k)}\rangle = \sqrt{\overline{(\mathbf{M}_{(k)} - \mathbf{M}_{(0)})\circ(\mathbf{M}_{(k)} - \mathbf{M}_{(0)})}}. \tag{12}$$

Here $\circ$ is the Hadamard product, denoting element-wise multiplication (i.e., each element of $(\mathbf{M}_{(k)} - \mathbf{M}_{(0)})$ is squared), and the overbar symbol, $\bar{}$, denotes the mean of the matrix elements. The overall error, $\langle\delta\mathbf{M}\rangle$, associated with the set is then the average of all $\langle\delta\mathbf{M}_{(k)}\rangle$:

$$\langle\delta\mathbf{M}\rangle = \frac{\sum_{k=1}^{160}\langle\delta\mathbf{M}_{(k)}\rangle}{160}. \tag{13}$$

Results are summarized in Fig. 4. As predicted, the Optimum set allowed for the most robust Mueller matrix determination. The error associated with the Optimum set is significantly lower than that of all other sets, as determined by two-tailed unpaired t-tests ($p < 0.05$).

The error associated with the Rotated-Optimum set is close to, but significantly greater than that associated with the Optimum set ($p = 0.02$). This highlights the effect of phase errors on Mueller matrix determination, as these sets only differ in their orientation on the Poincaré sphere.

Furthermore, the error associated with Rotated-Optimum is lower than, but not statistically different ($p > 0.05$) from, Random1. The similarity between these sets illustrates how phase errors and input vector "spread" must be considered when choosing input states. Even though Random1 vectors do not form a platonic solid, they do avoid the phase-error regions to a greater extent than the Rotated-Optimum vectors. Thus it appears the advantage of Rotated-Optimum's cubic configuration is negated by its proximity to phase-error regions.

It is interesting that Random1 allows for more robust Mueller matrix determination than Random2, despite being further from a cubic configuration, as evidenced by its smaller mean separation angle. As in the previous case, this is likely because Random1 avoids the phase-error regions better than Random2.

Finally, Random3 resulted in the least robust Mueller matrix determination. This is expected as it had the smallest mean separation angle and, of all Random sets, the most Stokes vectors near the phase-error regions.

This study is limited, as our evaluation of Mueller matrix determination "robustness" is only based on the precision (or repeatability) afforded by the different sets of input Stokes vectors, not their accuracy. This was done because, to assess accuracy, the "true" Mueller matrix of the sample would need to be known to a great degree of exactness, which is a difficult challenge with a biological phantom. Furthermore, there are infinite possible sets of input Stokes vectors, but testing an increasingly large number becomes impractical. Nevertheless, this study, in combination with previous work [14], offers confidence in the optimum input polarizations.

In conclusion, we have experimentally validated that the spread of input polarization vectors and their proximity to phase-error regions must be considered when performing Mueller matrix polarimetry with a dual PEM setup. We also have provided experimental evidence that the set of Stokes vectors forming a cube on the Poincaré sphere, with vertices oriented as far away as possible from phase-error regions, allows for the most robust Mueller matrix determination with a dual-PEM polarimeter.

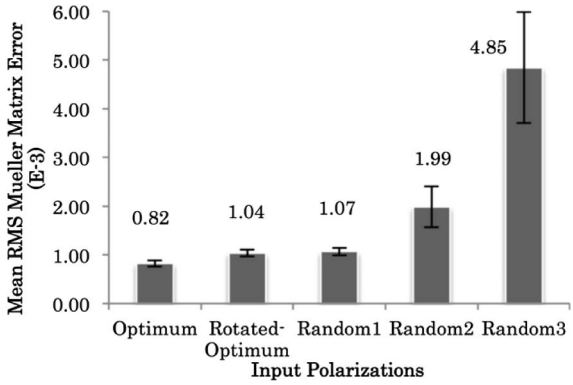

Fig. 4. Mueller matrix error associated with different sets of input Stokes vectors. Error bars show standard error. Differences between all sets were significant, as determined by two-tailed unpaired t-tests ($p < 0.05$), except between Rotated-Optimum and Random1. Optimum allows the most robust Mueller matrix determination, since its vectors are evenly spread about the Poincaré sphere and are maximally distant from phase-error regions.

Support from the Natural Sciences and Engineering Research Council of Canada is gratefully acknowledged.

References

1. G. G. Stokes, Trans. Cambridge Philos. Soc. **9**, 399 (1852).
2. H. Poincaré, *Theorié Mathématique de la Lumière* (Gauthiers-Villars, 1892).
3. D. S. Kliger, J. W. Lewis, and C. E. Randall, *Polarized Light in Optics and Spectroscopy* (Academic–Harcourt Brace Jovanovich, 1990).
4. N. Ghosh and I. A. Vitkin, J. Biomed. Opt. **16**, 110801 (2011).
5. D. Côté and I. A. Vitkin, J. Biomed. Opt. **9**, 213 (2004).
6. N. Ghosh, M. F. G. Wood, S. Li, R. D. Weisel, B. C. Wilson, R.-K. Li, and I. A. Vitkin, J. Biophoton. **2**, 145 (2009).
7. M. F. G. Wood, N. Ghosh, M. A. Wallenburg, S.-H. Li, R. D. Weisel, B. C. Wilson, R.-K. Li, and I. A. Vitkin, J. Biomed. Opt. **15**, 047009 (2010).
8. S. Alali, Y. Wang, and I. A. Vitkin, Biomed. Opt. Express **3**, 3250 (2012).
9. S. Alali, K. J. Aitken, A. Shröder, D. J. Bagli, and I. A. Vitkin, J. Biomed. Opt. **17**, 086010 (2012).
10. A. Pierangelo, A. Nazac, A. Benali, P. Validire, H. Cohen, T. Novikova, B. H. Ibrahim, S. Manhas, C. Fallet, M. R. Antonelli, and A. De Martino, Opt. Express **21**, 14120 (2013).
11. A. Pierangelo, A. Benali, M. R. Antonelli, T. Novikova, P. Validire, B. Gayet, and A. De Martino, Opt. Express **19**, 1582 (2011).
12. P. A. Letnes, I. S. Nerbø, L. M. S. Aas, P. G. Ellingsen, and M. Kildemo, Opt. Express **18**, 23095 (2010).
13. W. Guan, G. A. Jones, Y. Liu, and T. H. Shen, J. Appl. Phys. **103**, 043104 (2008).
14. D. Layden, M. F. G. Wood, and I. A. Vitkin, Opt. Express **20**, 20466 (2012).
15. S. Alali, M. Ahmad, A. J. Kim, M. F. G. Wood, and I. A. Vitkin, J. Biomed. Opt. **17**, 045004 (2012).